

# CO Poisoning of Ru Catalysts in CO<sub>2</sub> Hydrogenation under Thermal and Plasma Conditions: A Combined Kinetic and Diffuse Reflectance Infrared Fourier Transform Spectroscopy–Mass Spectrometry Study

Shanshan Xu, Sarayute Chansai, Shaojun Xu, Cristina E. Stere, Yilai Jiao, Sihai Yang, Christopher Hardacre,\* and Xiaolei Fan\*



Cite This: *ACS Catal.* 2020, 10, 12828–12840



Read Online

ACCESS |



Metrics & More



Article Recommendations

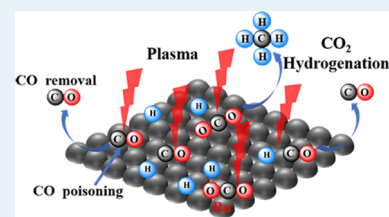


Supporting Information

**ABSTRACT:** Plasma-catalysis systems are complex and require further understanding to advance the technology. Herein, CO poisoning in CO<sub>2</sub> hydrogenation over supported ruthenium (Ru) catalysts in a nonthermal plasma (NTP)-catalysis system was investigated by a combined kinetic and diffuse reflectance infrared Fourier transform spectroscopy–mass spectrometry (DRIFTS–MS) study and compared with the thermal catalytic system. The relevant findings suggest the coexistence of the Langmuir–Hinshelwood and Eley–Rideal mechanisms in the NTP-catalysis. Importantly, comparative study of CO poisoning of the Ru catalyst was performed under the thermal and NTP conditions, showing the advantage of the hybrid NTP-catalysis system over the thermal counterpart to mitigate CO poisoning of the catalyst.

Specifically, compared with the CO poisoning in thermal catalysis due to strong CO adsorption and associated metal sintering, *in situ* DRIFTS–MS analysis revealed that the collisions of reactive plasma-derived species in NTP-catalysis could remove the strongly adsorbed carbon species to recover the active sites for CO<sub>2</sub> activation. Thus, the NTP-catalysis was capable of preventing CO poisoning of the Ru catalyst in CO<sub>2</sub> hydrogenation. Additionally, under the NTP conditions, the NTP-enabled water-gas shift reaction of CO with H<sub>2</sub>O (which was produced by CO/CO<sub>2</sub> hydrogenation) shifted the equilibrium of CO<sub>2</sub> hydrogenation toward CH<sub>4</sub> production.

**KEYWORDS:** nonthermal plasma (NTP) catalysis, CO poisoning, Ru catalyst, CO<sub>2</sub> hydrogenation, kinetics, DRIFTS–MS



## 1. INTRODUCTION

Hybrid nonthermal plasma (NTP) and catalysis (NTP-catalysis) systems can activate and convert a variety of stable molecules, such as carbon dioxide (CO<sub>2</sub>), methane (CH<sub>4</sub>), and nitrogen (N<sub>2</sub>), into desired products under mild conditions, e.g., ambient pressure and low bulk gas temperatures (<200 °C),<sup>1–3</sup> but the hybrid system is highly complex. NTP-catalysis is particularly beneficial to enable kinetically and/or thermodynamically limited reactions, including dry reforming of methane,<sup>4</sup> water-gas shift,<sup>5,6</sup> and CO<sub>2</sub> hydrogenation.<sup>7</sup> In comparison with the thermal counterparts, NTP-catalysis has shown the capability of lowering the energy barrier required for the catalysis and/or changing the reaction pathways on the catalyst surface.<sup>8,9</sup> Recent studies have shown that, being similar with the thermal catalysis, the intrinsic nature of heterogeneous catalysts (including the supports), such as metal dispersion and pore structure, plays a key role in NTP-catalysis. For example, a series of Ni supported on silicalite-1 (with different pore structures) catalysts was designed to study CO<sub>2</sub> hydrogenation under NTP conditions. It was found that the pore structure of the silicalite-1 supports determines the dispersion and location of Ni sites and, hence, the accessibility of plasma-generated reactive species, thus affecting the performance of the NTP-catalysis.<sup>10</sup>

In addition to the activity, the stability and longevity of the catalysts are important factors for practical catalysis under both thermal and NTP conditions. Under thermal conditions during CO<sub>2</sub> hydrogenation, catalyst deactivation is mainly caused by (i) metal particle sintering due to high reaction temperatures, (ii) coking caused by carbon deposition, and (iii) catalyst poisoning resulting from trace impurities in the feed gases such as carbon monoxide (CO). Due to the low-temperature activation of catalytic process, NTP-assisted CO<sub>2</sub> hydrogenation intrinsically avoids sintering and coking processes.<sup>9</sup> Regarding catalyst poisoning, specifically CO<sub>2</sub> hydrogenation, it is well known that CO poisoning is one of the worst catalyst-deactivating processes under thermal conditions.<sup>11,12</sup> Under plasma conditions, conversely, previous studies have shown that the plasma could enable the recovery of poisoned catalytic sites *via* dynamic collisions among reactive plasma-derived species, which lead to the desorption of strongly bound surface species.<sup>13,14</sup> Accordingly, insights into CO poisoning under

Received: August 18, 2020

Revised: October 8, 2020

thermal and NTP conditions, especially relevant deactivation mechanisms, need to be assessed to develop mature NTP-catalysis technology for potential practical adoptions. NTP-catalysis is a complex combination of plasma discharge and surface reactions (and other factors) with multifaceted interplays between them. Regarding the surface reactions under NTP conditions, *in situ* techniques, such as diffuse reflectance infrared Fourier transform (DRIFTS)<sup>7,9</sup> and extended X-ray absorption fine structure (EXAFS) spectroscopy,<sup>15</sup> have been proved to be powerful tools to gain insights into the surface dynamics of the catalyst, reaction mechanisms, and the catalyst state during NTP-catalysis, which can facilitate the rational design of bespoke catalysts for NTP conditions. However, relevant *in situ* studies of NTP-catalysis toward the understanding of catalyst poisoning are still lacking.

This work presents the comparative study of the effect of CO on CO<sub>2</sub> hydrogenation over a supported Ru catalyst (*i.e.*, CO poisoning) under thermal and NTP conditions. The intrinsic nature of the catalysts on the performance of CO<sub>2</sub> hydrogenation was first studied, and the Ru/SiO<sub>2</sub> catalyst with high activity and stability was chosen for further investigation. To elucidate the mechanism of CO poisoning, the mechanistic investigation of CO<sub>2</sub> hydrogenation including the kinetic and *in situ* DRIFTS studies was comparatively performed under thermal and NTP conditions, which provide useful information on the intermediates and reaction pathways of CO<sub>2</sub> hydrogenation. Finally, the mechanism of CO poisoning in CO<sub>2</sub> hydrogenation over the Ru/SiO<sub>2</sub> catalyst was investigated. Under the thermal conditions, significant catalyst deactivation due to the strong CO adsorption and metal sintering was observed; conversely, NTP activation was found to mitigate the effect of CO on the performance of the catalyst and regenerate the catalyst efficiently.

## 2. EXPERIMENTAL SECTION

### 2.1. Preparation and Characterization of Catalysts.

Ruthenium (III) chloride trihydrate (RuCl<sub>3</sub>·3H<sub>2</sub>O), silicon dioxide, and  $\gamma$ -Al<sub>2</sub>O<sub>3</sub> were purchased from Sigma-Aldrich and used without further purification.

Supported Ru catalysts including Ru/SiO<sub>2</sub> and Ru/ $\gamma$ -Al<sub>2</sub>O<sub>3</sub> (with the theoretical metal loading of 2 wt %) were prepared using the wet impregnation method. First, the support (1.5 g) was suspended in water (30 mL), and then 6.2 mL of RuCl<sub>3</sub>·3H<sub>2</sub>O solution (10 mg mL<sup>-1</sup>) was added dropwise. The mixture was vigorously stirred for 3 h and then evaporated using a rotary evaporator. The resulting precipitate was dried at 70 °C in a convection oven for 12 h. The obtained dry solid was subsequently reduced in pure H<sub>2</sub> at 300 °C for 2 h with a heating rate of 5 °C min<sup>-1</sup>. After reduction, the sample was cooled down to room temperature (RT) naturally under the H<sub>2</sub> flow (at 100 mL min<sup>-1</sup>). The actual metal loading was determined by inductively coupled plasma optical emission spectrometry (ICP-OES; [Supporting information](#)). The prepared catalysts were characterized to understand their physical and chemical properties by bright-field transmission electron microscopy (TEM), N<sub>2</sub> physisorption (using the Brunauer–Emmett–Teller (BET) method), hydrogen temperature programmed reduction (H<sub>2</sub>-TPR), and CO chemisorption, and the relevant experimental details are provided in the [Supporting Information](#).

**2.2. Catalysis.** A dielectric barrier discharge (DBD) flow reactor was used for NTP-activated CO<sub>2</sub> hydrogenation, which is depicted in [Figure S1](#), and the details of the DBD reactor

have been described elsewhere.<sup>9</sup> Parameters of the NTP-catalysis system were measured using an oscilloscope (Tektronix TBS1072B) connected with a high-voltage probe (Tektronix, P6015) and current monitor. NTP-catalysis was performed at atmospheric pressure without a heating source. Briefly, ~100 mg of catalyst (pellet sizes of 250–425  $\mu$ m) was packed into a quartz tube (6 mm o.d.  $\times$  4 mm i.d.), where an aluminum foil wrapped outside of the tube served as the high-voltage electrode and a tungsten rod (1 mm o.d.) in the center of reactor acted as the ground electrode. Since the catalyst was exposed to air at RT before being loaded to the DBD reactor, it was treated *in situ* by NTP (at 6.5 kV) using 50% H<sub>2</sub>/Ar as the discharge gas for 20 min before catalysis. The feed of CO<sub>2</sub>, H<sub>2</sub>, and Ar balance (molar ratio of 1:3:3) was introduced by mass flow controllers (Bronkhorst, F-201CV-500-RAD-11-V) with the flowrate of 50 mL min<sup>-1</sup>. The applied voltage was from 5.5 to 7.5 kV at a constant frequency of 21.0 kHz. The product was analyzed by using online mass spectrometry (MS, Hidden HPR-20) and two-channel online gas chromatography (GC) equipped with a Porapak Q packed column, thermal conductivity detector (TCD), and flame ionization detector (FID). An Ar balance was used in the system to avoid the signal saturation of MS signal. For each measurement, three samples of gas products were analyzed under steady-state conditions for an average value and error determination. Control experiments using the empty reactor (catalyst-free) and the reactor with the bare supports as a packing were performed under the same NTP conditions.

CO poisoning study under the NTP condition (at 6.5 kV and 21.0 kHz) was investigated by varying the inlet molar ratio of CO/CO<sub>2</sub> between 0 and 2. The total gas feed flowrate was 50 mL min<sup>-1</sup>, corresponding to a space velocity of 30,000 mL (STP) g<sub>cat</sub><sup>-1</sup> h<sup>-1</sup>, which included CO<sub>2</sub>, CO, H<sub>2</sub>, and Ar balance (molar ratio of H<sub>2</sub>/(CO<sub>2</sub> + CO) = 3). Catalyst deactivation was monitored as a function of time-on-stream (ToS) by switching the CO on and off in the feed. The average bulk temperature of the system between 5.5 and 7.5 kV was measured using an infrared (IR) thermometer and was in the range of 110–135 °C. Specifically, the average bulk temperature at 6.5 kV was ~129 °C, which could not activate CO<sub>2</sub> conversion thermally, according to a previous study.<sup>9</sup>

For comparison, thermal catalysis was carried out at 250–430 °C at atmospheric pressure. Prior to catalysis, the catalyst (pellets, about 100 mg) was first treated at 300 °C for 1 h in 50% H<sub>2</sub>/Ar. Then, the feed (CO<sub>2</sub>/H<sub>2</sub>/Ar = 1:3:3) was introduced into the reactor at 50 mL min<sup>-1</sup>. The temperature of the catalyst bed was monitored by a K-type thermocouple embedded in the catalyst bed.

CO poisoning of the catalyst under the thermal condition (at 330 °C) was studied using the same gas condition as in the relevant NTP-catalysis. The catalyst deactivation experiment was performed at 330 °C with the same gas conditions as described in the NTP-catalysis (for CO poisoning study).

CO<sub>2</sub> ( $X_{\text{CO}_2}$ ) conversion, CO ( $X_{\text{CO}}$ ) conversion, carbon ( $X_{\text{C}} = X_{\text{CO}_2} + X_{\text{CO}}$ ) conversion, selectivity toward CH<sub>4</sub> ( $S_{\text{CH}_4}$ ), and CH<sub>4</sub> yield ( $Y_{\text{CH}_4}$ ) were determined accordingly to evaluate the catalytic performance (all the performance parameters are defined in the [Supporting Information](#)).

**2.3. Kinetic Study.** The kinetic study of thermal catalysis was performed at 260–320 °C with ~30 mg of catalyst (diluted with inert glass beads to prevent hot spots) to ensure low CO<sub>2</sub> conversions of <20%. The feed mixture containing

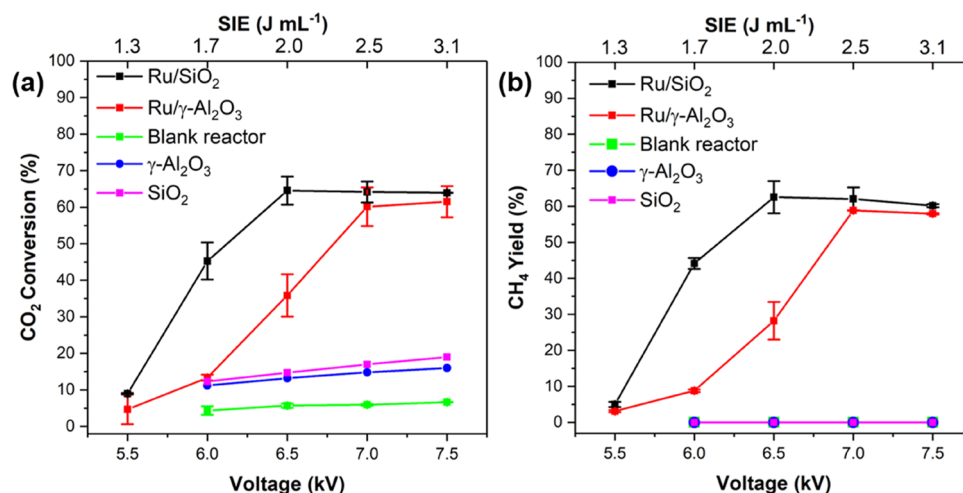


**Figure 1.** Performance of NTP-activated catalytic CO<sub>2</sub> hydrogenation as a function of voltage/input energy over the Ru/SiO<sub>2</sub> and Ru/γ-Al<sub>2</sub>O<sub>3</sub> catalysts in reference to the control experiments; (a) CO<sub>2</sub> conversion and (b) CH<sub>4</sub> yield. Experimental conditions: feed gas composition of CO<sub>2</sub>/H<sub>2</sub>/Ar = 1:3:3 and WHSV of 30,000 mL (STP) g<sub>cat</sub><sup>-1</sup> h<sup>-1</sup>.

CO<sub>2</sub>/H<sub>2</sub>/Ar (molar ratio = 1:3:3) was fed into the reactor for the kinetic study. To extract the reaction order with respect to H<sub>2</sub> and CO<sub>2</sub> partial pressures, the composition of the feed was varied; *i.e.*, H<sub>2</sub> partial pressure was changed with a constant partial pressure of CO<sub>2</sub> and vice versa.

Kinetic study of the NTP-catalysis was performed using similar procedures and conditions as described above (about 30 mg of catalyst diluted with glass beads, at 5.0–6.5 kV and 21.0 kHz). The gas conditions were the same as in the kinetic study of the thermal catalysis. Due to the low bulk temperature under the NTP conditions (<129 °C), thermal activation of CO<sub>2</sub> was not possible. Considering the effect of support packing and discharge volume, control experiments using the same amount of the bare supports and inert glass beads were performed to extract the information on the relevant gas phase and surface (over the bare supports) reactions under NTP, which was subsequently used to correct the kinetic data of the NTP-catalysis (Supporting Information).

**2.4. In Situ DRIFTS–MS.** The experimental setup of DRIFTS–MS for NTP-catalysis was described elsewhere.<sup>9</sup> The catalyst was pretreated with 50% H<sub>2</sub>/Ar gas under NTP at 6.0 kV and 27.0 kHz for 20 min in the flow cell. Then, the gas mixture containing CO<sub>2</sub>, CO, H<sub>2</sub>, and Ar balance was fed into the cell for the reaction. Kr at 10 mL min<sup>-1</sup> was also introduced as the internal standard. The use of Ar balance in DRIFTS experiments was to avoid the signal saturation of IR spectra and MS signal. NTP-catalysis in the DRIFTS cell was performed at a constant peak voltage of 5.5 kV to avoid arcing between the electrodes. The IR spectra were recorded every 60 s with a resolution of 4 cm<sup>-1</sup> and analyzed by OPUS software.

### 3. RESULTS AND DISCUSSION

**3.1. Effect of Catalysts in the NTP-Catalysis.** CO<sub>2</sub> hydrogenation over the two supported Ru catalysts under NTP conditions was investigated in reference to the control experiments (*i.e.*, the empty tube for NTP-alone experiments and the reactor with the bare γ-Al<sub>2</sub>O<sub>3</sub> and SiO<sub>2</sub> support packing under the NTP conditions) to screen the candidate for the following study (as shown in Figure 1). Under the NTP conditions without a catalyst, CO<sub>2</sub> was decomposed to CO with a trivial conversion of ~6% at 6.5 kV (with the specific input energy (SIE) of 2.0 J mL<sup>-1</sup>). Similarly, NTP systems

with the bare γ-Al<sub>2</sub>O<sub>3</sub> and SiO<sub>2</sub> supports were only selective to CO with relevant CO<sub>2</sub> conversions of ~13 and ~15%, respectively, at 6.5 kV. In comparison with the system without a packing, that is, the blank experiment with an empty tube, the higher CO<sub>2</sub> conversions with the bare supports can be attributed to the enhanced average electric field strength, benefiting CO<sub>2</sub> dissociation.<sup>16</sup> Conversely, in NTP-catalysis with the voltage above 7.0 kV (SIE > 2.5 J mL<sup>-1</sup>), regardless of the Ru catalysts used in this work, CO<sub>2</sub> conversion and CH<sub>4</sub> yield increased significantly to >57%. However, Ru catalysts based on different supports showed different behaviors under the NTP conditions, demonstrating the effect of catalyst design on NTP-catalysis.<sup>17</sup> Specifically, the Ru/SiO<sub>2</sub> catalyst showed a higher activity as compared with the Ru/γ-Al<sub>2</sub>O<sub>3</sub> catalyst, especially at the lower voltage of <6.5 kV (SIE < 2.5 J mL<sup>-1</sup>). The highest CO<sub>2</sub> conversion (~65%) and CH<sub>4</sub> yield (~63%) at 6.5 kV were achieved by Ru/SiO<sub>2</sub>, while the Ru/γ-Al<sub>2</sub>O<sub>3</sub> catalyst only showed about 35% CO<sub>2</sub> conversion and 29% CH<sub>4</sub> yield, being less active for NTP-activated CO<sub>2</sub> hydrogenation. Similarly, under thermal conditions (Figure S2), Ru/SiO<sub>2</sub> outperformed Ru/γ-Al<sub>2</sub>O<sub>3</sub> as well, suggesting that the intrinsic nature of catalysts dominated the performance of CO<sub>2</sub> hydrogenation regardless of the means of activation. In detail, the corresponding TEM and CO chemisorption analysis of the Ru/SiO<sub>2</sub> and Ru/γ-Al<sub>2</sub>O<sub>3</sub> catalysts (Figure S3 and Table S3) showed that the two catalysts presented similar average particle sizes and Ru dispersions. Additionally, the metal–support interaction of the two catalysts was also similar, as revealed by H<sub>2</sub>-TPR (Figure S5). These findings show that the property of the supported active Ru phases of the two catalysts under study is similar, thus suggesting that the supported Ru might not affect the activity of the two catalysts significantly under NTP conditions.

Under NTP conditions, the effect of dielectric property of the bare supports on the catalysis was deemed insignificant since γ-Al<sub>2</sub>O<sub>3</sub> and SiO<sub>2</sub> have different dielectric constants (~9.1 and ~4.2, respectively), while the reaction results were similar.<sup>18</sup> In addition to the dielectric constant, the porous property of the packing material can also influence the plasma discharge and reaction performance under the NTP conditions.<sup>19</sup> N<sub>2</sub> physisorption analysis showed that the Ru/SiO<sub>2</sub> catalyst and Ru/γ-Al<sub>2</sub>O<sub>3</sub> catalyst had comparable pore volumes

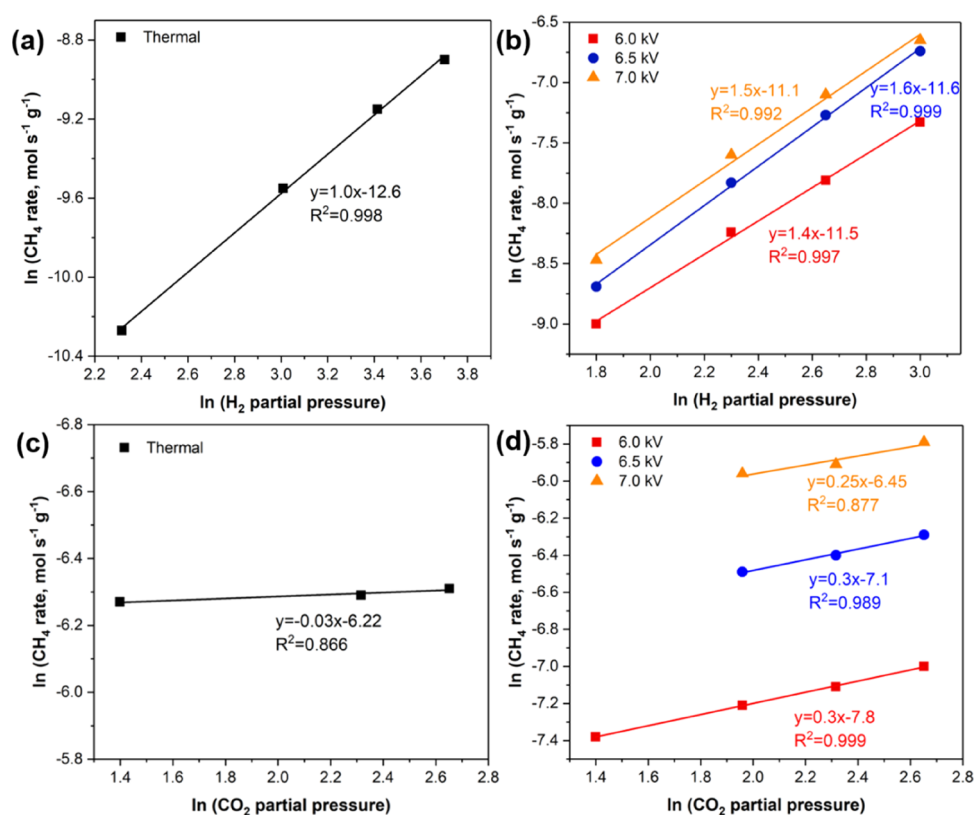


**Figure 2.** Dependence of the reaction rate on  $p_{\text{H}_2}$  and  $p_{\text{CO}_2}$  under (a, c) thermal conditions (at 330 °C) and (b, d) NTP conditions.

of  $\sim 0.7 \text{ cm}^3 \text{ g}^{-1}$ . The average pore sizes of the Ru/SiO<sub>2</sub> catalyst and Ru/ $\gamma$ -Al<sub>2</sub>O<sub>3</sub> catalyst were  $\sim 5$  and  $\sim 12$  nm, respectively, which are much smaller than the Debye length, suggesting that the penetration of plasma into the catalyst pores might be limited. However, a previous study based on Monte Carlo calculation revealed that microdischarges might be formed near the pores of mesoporous catalysts with mesopore sizes of 2–50 nm, and the relatively high surface area promoted the intensified surface discharge on the surface.<sup>20</sup> This may explain the better catalytic performance of Ru/SiO<sub>2</sub> in CO<sub>2</sub> hydrogenation than Ru/ $\gamma$ -Al<sub>2</sub>O<sub>3</sub> since the high surface area might promote the surface discharge in NTP-catalysis. The Ru/SiO<sub>2</sub> catalyst has a well-developed micro/mesoporous structure with a higher specific BET surface area of 557 m<sup>2</sup> g<sup>-1</sup> than that of the Ru/ $\gamma$ -Al<sub>2</sub>O<sub>3</sub> catalyst (239 m<sup>2</sup> g<sup>-1</sup>). Thus, a high surface area is expected as the key to determine the catalytic performance of the supported Ru catalysts under NTP and thermal conditions. The calculated apparent activation energy (Figure S6) showed that the Ru/SiO<sub>2</sub> catalyst presented lower values, under both conditions, than the Ru/ $\gamma$ -Al<sub>2</sub>O<sub>3</sub> catalyst (Table S4), e.g., 20 kJ mol<sup>-1</sup> versus 71 kJ mol<sup>-1</sup> in NTP-catalysis (details of the kinetic calculations are presented in the Supporting Information).<sup>8,9</sup>

**3.2. Comparative Mechanistic Study of CO<sub>2</sub> Hydrogenation over Ru/SiO<sub>2</sub>.** Preliminary catalytic assessments have shown that the Ru/SiO<sub>2</sub> catalyst presented relatively high CO<sub>2</sub> conversion and CH<sub>4</sub> yield for CO<sub>2</sub> hydrogenation under NTP and thermal conditions (in comparison with the Ru/ $\gamma$ -Al<sub>2</sub>O<sub>3</sub> catalyst); thus, the Ru/SiO<sub>2</sub> catalyst was selected for further investigation. To gain insight into the mechanism of CO poisoning in CO<sub>2</sub> conversions, first, the comparative mechanistic study of CO<sub>2</sub> hydrogenation over the Ru/SiO<sub>2</sub> catalyst was performed. Figure 2 and Table 1 show correlation

**Table 1.** Reaction Order with Respect to  $p_{\text{H}_2}$  and  $p_{\text{CO}_2}$  for Catalytic CO<sub>2</sub> Hydrogenation over Ru/SiO<sub>2</sub> under the Thermal (at 330 °C) and NTP Conditions

reaction order	NTP			thermal
	6.0 kV	6.5 kV	7.0 kV	
$p_{\text{H}_2}$	1.40	1.60	1.50	1.0
$p_{\text{CO}_2}$	0.30	0.30	0.25	-0.03

between the apparent reaction rate and the CO<sub>2</sub>/H<sub>2</sub> partial pressures ( $p_{\text{H}_2}$  and  $p_{\text{CO}_2}$ ) in CO<sub>2</sub> hydrogenation under the thermal and NTP conditions. Under the thermal condition at 330 °C, the CH<sub>4</sub> formation rate over the Ru/SiO<sub>2</sub> catalyst showed a stronger dependence on  $p_{\text{H}_2}$  than  $p_{\text{CO}_2}$  in the feed. Specifically, the reaction order with respect to  $p_{\text{H}_2}$  was calculated as 1.0, in line with the Langmuir–Hinshelwood mechanism.<sup>21</sup> A previous study showed that H<sub>2</sub> dissociation on the Ru surface was fast with the produced H<sub>ad</sub> being short-lived,<sup>22</sup> and the reaction order regarding  $p_{\text{H}_2}$  indicated that CO<sub>2</sub> and H<sub>2</sub> were adsorbed on the different active sites on the Ru surface.<sup>23,24</sup> The reaction order regarding  $p_{\text{CO}_2}$  was found to be -0.03, which can be approximated as zero order, suggesting that CO<sub>2</sub> concentration has a relatively weak influence on the formation rate of CH<sub>4</sub>. This finding suggested (i) the CO<sub>2</sub> chemisorption on the catalyst and (ii) the saturation of relevant active sites on the Ru surface by CO<sub>2</sub> molecules at relatively low CO<sub>2</sub> concentrations.<sup>22</sup> Therefore, under the thermal condition, CO<sub>2</sub> participated in the reaction *via* the Langmuir–Hinshelwood mechanism, *i.e.*, CO<sub>2</sub> adsorbed on the

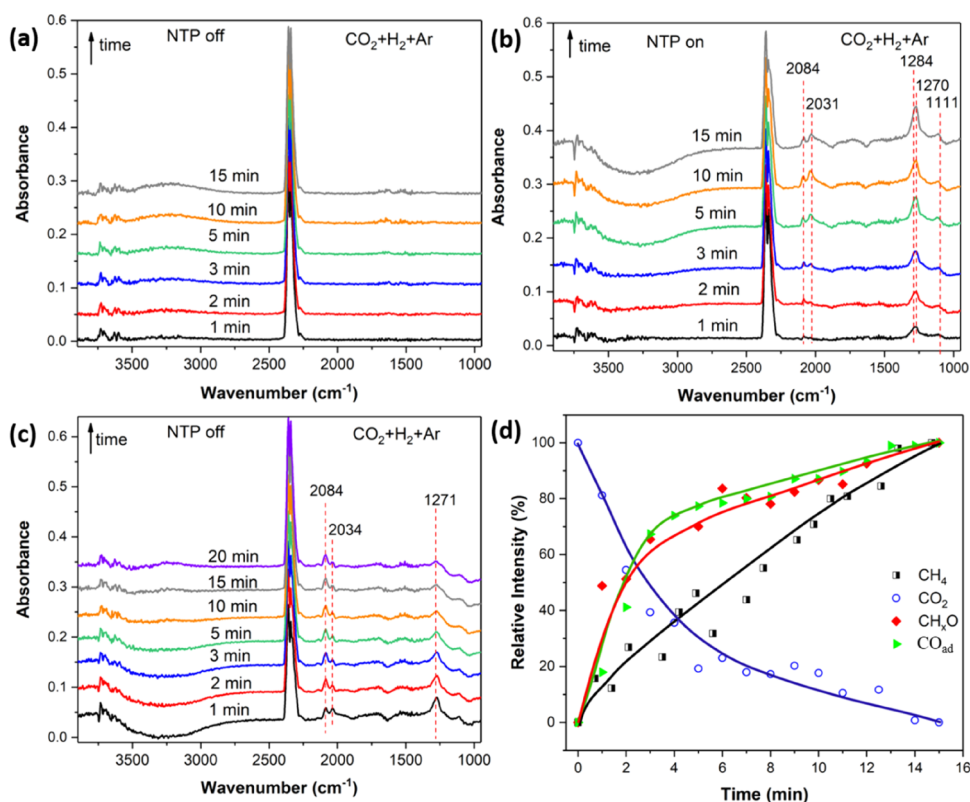


**Figure 3.** *In situ* DRIFTS spectra of surface species for CO<sub>2</sub> hydrogenation over the Ru/SiO<sub>2</sub> catalyst under (a) the NTP-off condition with the feed gas of 3% CO<sub>2</sub> + 9% H<sub>2</sub> + Ar, (b) NTP-on condition with the feed gas (at 5.5 kV and 27.0 kHz), and (c) NTP-off condition with the feed gas. (d) Relative intensities of surface species as a function of time-on-stream recorded by *in situ* DRIFTS from (b) and relative intensity change of methane recorded in MS (Figure S9) during CO<sub>2</sub> hydrogenation by NTP activation (at 5.5 kV and 27.0 kHz).

catalyst, and then dissociated to active intermediates under heating, which further react with H<sub>ad</sub> to form methane.

In comparison, under the NTP conditions, the reaction orders with respect to  $p_{\text{H}_2}$  and  $p_{\text{CO}_2}$  were  $1.50 \pm 0.10$  and  $0.30 \pm 0.05$ , respectively. Additionally, both reaction orders remained almost constant as a function of the input power, suggesting the same surface reaction mechanism at different input powers. The comparatively strong dependence on  $p_{\text{H}_2}$  and  $p_{\text{CO}_2}$  under NTP conditions (compared with the thermal condition) indicates the presence of multiple reaction pathways for CO<sub>2</sub> hydrogenation in NTP-catalysis. In addition to the surface reactions under the thermal catalysis, the vibrationally activated and dissociated active species (e.g., electronically excited H radical) in the gas-phase reaction under NTP conditions might also participate in the surface hydrogenation reactions *via* the Eley–Rideal mechanism.<sup>25</sup> To clarify the relationship between the reaction order and reaction mechanism under NTP and thermal conditions, *in situ* DRIFTS–MS was performed, and the relevant results were correlated with the kinetic data.

*In situ* DRIFTS coupled with MS characterization of CO<sub>2</sub> hydrogenation over the Ru/SiO<sub>2</sub> catalyst was comparatively performed under thermal and NTP conditions to investigate the mechanism of CO<sub>2</sub> hydrogenation. Under the thermal condition at 250 °C (Figure S7), characteristic peaks of surface hydroxyls (OH<sub>ad</sub>, from ~3596 to ~3730 cm<sup>-1</sup>), CH<sub>x</sub> species (CH<sub>3,ad</sub>, at ~3015 cm<sup>-1</sup>), carbonyl (CO<sub>ad</sub>, at ~1997 cm<sup>-1</sup>), and surface-adsorbed CH<sub>4</sub> (at ~3047 cm<sup>-1</sup>) were detected on the catalyst surface. It was observed that after changing the

feed to inert Ar, the CO<sub>ad</sub> band decreased slowly (within 10 min, Figure S7b), whereas the intensity of methane decreased rapidly (Figure S7c), suggesting that the gradual decrease of CO<sub>ad</sub> band was only due to the desorption under the condition used. Conversely, when the feed was changed to H<sub>2</sub>, the intensity of CO<sub>ad</sub> band declined fast (within 2 min) with the associated rapid emergence of peak in the CH<sub>4</sub> signal, which gradually decreased after 2 min. This phenomenon confirms CO<sub>ad</sub> as the active intermediate, which further reacted with H<sub>2</sub> to produce CH<sub>4</sub>, being in line with the kinetic data discussed above (Figure 2). Under thermal conditions, catalytic CO<sub>2</sub> hydrogenation is commonly thought to proceed *via* a direct carbon–oxygen bond dissociation mechanism,<sup>26,27</sup> which involves the dissociation of CO<sub>2</sub> on the catalyst surface (to adsorbed CO<sub>ad</sub> and surface C) and the subsequent hydrogenation of surface C. Under the thermal condition used in this work, DRIFTS only probed CO<sub>ad</sub> species on the Ru surface, confirming the direct carbon–oxygen bond dissociation mechanism.

Under the NTP condition with a CO<sub>2</sub>/Ar mixture, the gas-phase CO<sub>2</sub> dissociation was confirmed, as shown in Figure S8. With the NTP on (Figure S8b), the linearly and bridged adsorbed CO<sub>ad</sub> species (at ~2092, 2041, and 1881 cm<sup>-1</sup>) and bidentate and monodentate carbonate (at ~1274 and ~1311 cm<sup>-1</sup>, respectively) were measured. Since carbonate species were not observed under the thermal condition, the presence of carbonate species under the NTP condition was due to the plasma excitation and could be ascribed to the adsorption of vibrationally excited CO<sub>2</sub> species on the catalyst surface.

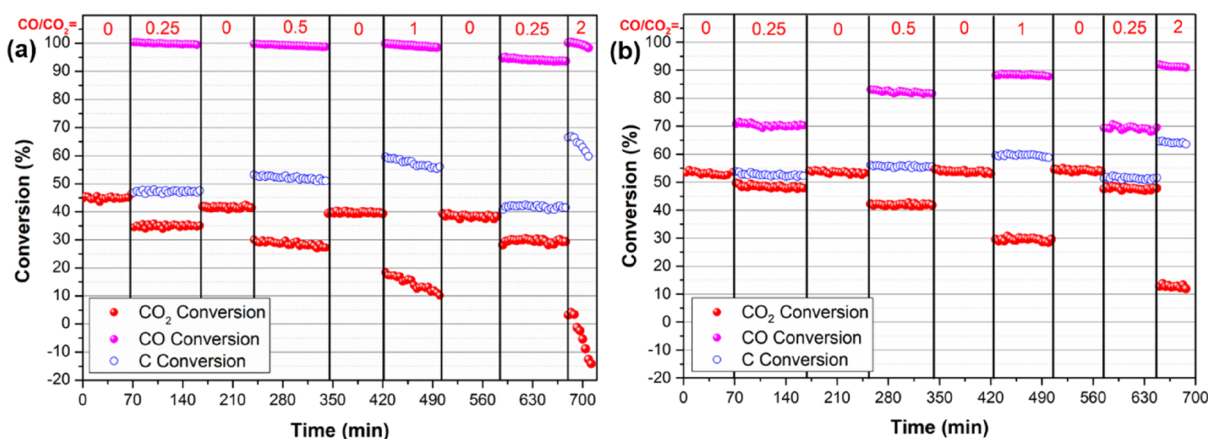


**Figure 4.** CO<sub>2</sub>, CO, and carbon conversions as a function of ToS in CO poisoning experiments with different CO/CO<sub>2</sub> inlet molar ratios under (a) thermal condition (at 330 °C) and (b) NTP condition (at 6.5 kV and 21.0 kHz).

Under the NTP-off condition, with the reaction gas feed (*i.e.*, 3% CO<sub>2</sub>/9% H<sub>2</sub>/Ar), in addition to the CO<sub>2</sub> gas-phase peak (at ~2360 and 2342 cm<sup>-1</sup>, as shown in Figure 3a), surface carbon species were not detected by DRIFTS and no reaction was observed (according to MS). Upon the ignition of plasma, the MS profile showed the instantaneous appearance of CH<sub>4</sub> signal (Figure S9a), confirming the formation of CH<sub>4</sub> over the catalyst under NTP activation. At the same time, surface formyl species (CH<sub>x</sub>O, at about 1284, 1270, and 1111 cm<sup>-1</sup>) and carbonyl species (*i.e.*, linearly adsorbed CO<sub>ad</sub> on Ru<sup>0</sup> at 2034 cm<sup>-1</sup> and linear form Ru<sup>δ+</sup>-CO at 2084 cm<sup>-1</sup>),<sup>28</sup> as shown in Figure 3b, were measured by DRIFTS. Compared with the CO<sub>ad</sub> bands formed under CO<sub>2</sub>/Ar (Figure S8b), the two peaks shifted toward lower frequency by about 10 cm<sup>-1</sup> and the bridged adsorbed CO<sub>ad</sub> peak disappeared, which could be attributed to the electron donation of H<sub>ad</sub> on the Ru surface.<sup>29</sup> On switching off the plasma, the CH<sub>4</sub> concentration decreased immediately (Figure S9), while the formyl species decreased slowly (within 4 min), indicating that the system without plasma discharge was inactive for CH<sub>4</sub> formation (Figure S9b). The gradual decrease of formyl band (within 4 min) reflects its desorption under the NTP-off condition. CO<sub>2</sub> hydrogenation can undergo the formyl pathway over Ru-based catalysts,<sup>30,31</sup> which involves the direct CO<sub>2</sub> dissociation to carbonyl (CO<sub>ad</sub>) and O<sub>ad</sub>, followed by the hydrogenation of CO<sub>ad</sub>. The subsequent hydrogenation of CO<sub>ad</sub> will form the formyl species as the intermediates for CH<sub>4</sub> production. As compared with the DRIFTS findings from the thermal system (*i.e.*, only carbonyl species were observed, Figure S7), the appearance of carbonyl species and formyl species under NTP conditions suggested the presence of an alternative reaction pathway (*i.e.*, formyl pathways) for CO<sub>2</sub> hydrogenation under NTP. Thus, evolution of the surface species as a function of ToS coupled with the change in CH<sub>4</sub> signal intensity (from MS) was correlated, as presented in Figure 3d. The CO<sub>ad</sub> species increased at a steeper rate than gas CH<sub>4</sub>, which could be explained by the plasma-assisted CO<sub>2</sub> dissociation in the gas phase and the dissociation of adsorbed CO<sub>2</sub> on the catalyst surface. The same phenomenon was found between the formation rates of surface formyl species and CH<sub>4</sub>, indicating CH<sub>x</sub>O species originating from reactions between CO<sub>ad</sub> and H<sub>ad</sub> and as the surface intermediate for CH<sub>4</sub> production.<sup>30,32</sup> The findings of this work confirmed the presence of the formyl pathway in CO<sub>2</sub> hydrogenation over Ru/SiO<sub>2</sub> under NTP

conditions; *i.e.*, CO<sub>2</sub> was dissociated to CO<sub>ad</sub> and O<sub>ad</sub> species on the catalyst surface, then CO<sub>ad</sub> was hydrogenated with H<sub>ad</sub> into formyl intermediate (CH<sub>x</sub>O) species, and finally, the formyl group reacted toward CH<sub>4</sub> and H<sub>2</sub>O. In comparison with the thermally activated CO<sub>2</sub> hydrogenation, the vibrationally activated CO<sub>2</sub> molecules under NTP conditions could adsorb on the catalyst surface with lower energy barriers, which facilitated the formation of CO<sub>ad</sub> species.<sup>14</sup> This activation promoted the hydrogenation of CO<sub>2</sub> and formation rate of CH<sub>4</sub>, leading to the reaction order of *p*<sub>CO<sub>2</sub></sub> increasing slightly. Additionally, the plasma-induced excited/dissociated H radicals in the gas phase might also interact with the adsorbed species to form CH<sub>4</sub> (*i.e.*, the formyl pathway) *via* the Eley–Rideal mechanism in CO<sub>2</sub> hydrogenation under NTP.<sup>14,25</sup> Due to the relatively low dissociation energy of H<sub>2</sub> molecules (~4.5 eV),<sup>33</sup> the plasma could activate H<sub>2</sub> more efficiently, which produces more H radicals with an increase in H<sub>2</sub> concentration in the feed. Therefore, under NTP, the H<sub>2</sub> partial pressure has a significant influence on the formation rate of CH<sub>4</sub>, leading to a much higher reaction order with respect to *p*<sub>H<sub>2</sub></sub> than that in the thermal catalysis.

**3.3. Investigation of CO Poisoning on CO<sub>2</sub> Hydrogenation.** Catalyst deactivation is complex and significant for practical catalysis. As expected, under the NTP condition (at 6.5 kV, 21.0 kHz), the Ru/SiO<sub>2</sub> catalyst in CO<sub>2</sub> hydrogenation presented excellent stability over 27 h ToS with CO<sub>2</sub> conversions and CH<sub>4</sub> selectivity maintained at 64.7 ± 0.7% and 94.1 ± 0.3%, respectively (Figure S10). Comparative TEM analysis of the catalyst before and after the longevity test showed no significant change regarding the particle sizes, neither the sign of metal sintering, which confirmed the anticoking and antisintering performance of the NTP-catalysis (Figure S11).

In addition to coking and sintering, catalyst poisoning is another major factor to deactivate the catalyst. Accordingly, to understand CO poisoning in the catalysis under the thermal and plasma conditions, relevant experiments were performed by varying CO concentration in the gas feed, keeping the H<sub>2</sub>/C (*i.e.*, CO<sub>2</sub> + CO) inlet molar ratio constant. Figure 4 shows the thermal and NTP-activated carbon conversions (CO<sub>2</sub>, CO, and overall) as a function of ToS with different CO/CO<sub>2</sub> ratios in the feed gas. Under the thermal condition at 330 °C (Figure 4a), the fresh Ru/SiO<sub>2</sub> catalyst showed a stable CO<sub>2</sub> conversion (~47%) without CO in the feed gas (CO/CO<sub>2</sub> =

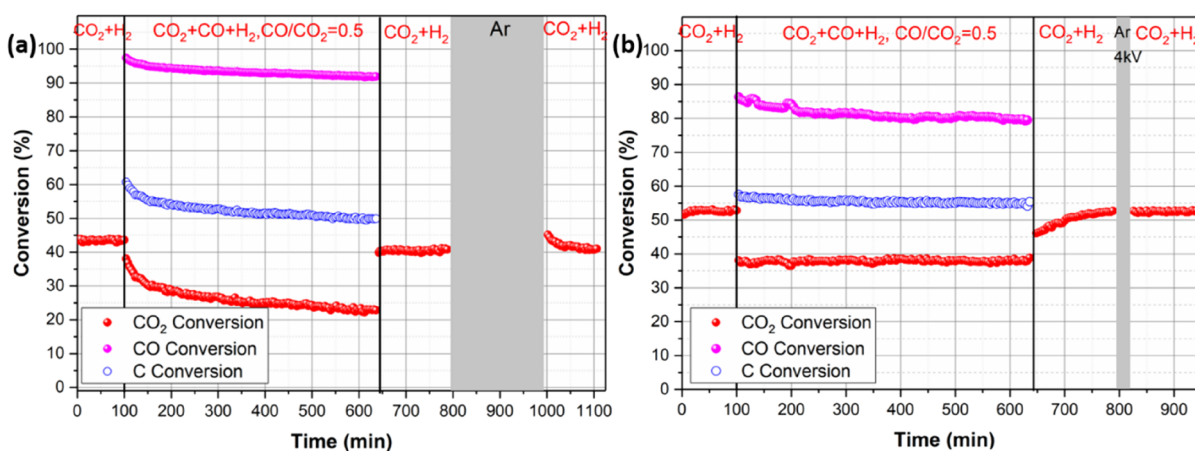


**Figure 5.** Long-term deactivation test with the  $\text{CO}_2/\text{CO}/\text{H}_2$  mixtures, regeneration treatment under Ar, and catalysis in  $\text{CO}_2/\text{H}_2$  over the Ru/SiO<sub>2</sub> catalyst under (a) the thermal condition (at 330 °C) and (b) NTP condition (at 6.5 kV and 21.0 kHz). Experimental conditions: feed gas composition of  $\text{H}_2/\text{C} = 3$ ,  $\text{CO}/\text{CO}_2 = 0.5$ , and WHSV of 30,000 mL (STP)  $\text{g}_{\text{cat}}^{-1} \text{h}^{-1}$ .

0, ToS = 0–70 min in Figure 4a). When CO ( $\text{CO}/\text{CO}_2 = 0.25$ ) was introduced in the gas mixture,  $\text{CO}_2$  conversion decreased to 35%, while CO was almost completely consumed, promoting the overall carbon conversion and  $\text{CH}_4$  production due to CO hydrogenation. By switching back to the “CO-free” feed gas ( $\text{CO}/\text{CO}_2 = 0$ , ToS = 165–240 min in Figure 4a), catalyst deactivation occurred, and the catalyst could not be fully recovered, as evidenced by the reduced  $\text{CO}_2$  conversion (Figure 4a) and  $\text{CH}_4$  production (Figure S12a), in comparison with that of the fresh catalyst. By further increasing the  $\text{CO}/\text{CO}_2$  ratio to 0.5 and 1.0, the decrease in  $\text{CO}_2$  conversion and deactivation of catalyst became more significant, while the CO conversion remained almost complete. The findings showed a strong inhibiting effect of CO on  $\text{CO}_2$  conversion. The condition with  $\text{CO}/\text{CO}_2 = 0.25$  in the feed gas (ToS = 590–680 min in Figure 4a) was tested again, and carbon conversion and  $\text{CH}_4$  production were lower than the previously measured values, suggesting the permanent deactivation of Ru/SiO<sub>2</sub>. By adding more CO in the feed (*i.e.*,  $\text{CO}/\text{CO}_2$  ratio of 2), severe CO poisoning was measured. Specifically, the  $\text{CO}_2$  conversion dropped rapidly below zero, suggesting that  $\text{CO}_2$  was formed in the system. This might be attributed to the presence of CO disproportionation ( $2\text{CO} \rightarrow \text{C} + \text{CO}_2$ )<sup>34</sup> and/or water-gas shift reaction (WGSR,  $\text{CO} + \text{H}_2\text{O} \rightarrow \text{H}_2 + \text{CO}_2$ )<sup>35</sup> due to the excessive CO in the feed and strong adsorption of CO on the Ru surface. Accordingly, in the thermal catalysis system, a decrease in  $\text{CO}_2$  conversion with CO cofeeding was not due to the kinetic effect, that is, the diluted  $\text{CO}_2$  concentration in the gas feed, as discussed above (Figure 2). With the presence of CO in the feed, competitive adsorption of CO and  $\text{CO}_2$  on metal active sites occurs.<sup>36</sup> Since the adsorption energy of CO (−2.3 eV) is much lower than that of  $\text{CO}_2$  (−0.52 eV),<sup>37</sup> preferential adsorption of CO and inhibited  $\text{CO}_2$  adsorption on the Ru surface are expected and, thus, a decrease in  $\text{CO}_2$  conversion. It was proposed that the formation of strongly adsorbed carbonyl species<sup>11,38</sup> due to the presence of CO might be the dominant factor for catalyst deactivation. Therefore, the mechanism of CO poisoning of the Ru/SiO<sub>2</sub> catalyst was investigated by *in situ* DRIFTS analysis (to be discussed later).

As shown in Figure 4b, under the NTP condition at 13.0 kV, 54%  $\text{CO}_2$  conversion over the Ru/SiO<sub>2</sub> catalyst was measured with the absence of CO in the feed (*i.e.*,  $\text{CO}/\text{CO}_2 = 0$ , ToS =

0–70 min, in Figure 4b). By introducing CO in the feed (with  $\text{CO}/\text{CO}_2 = 0.25$ ),  $\text{CO}_2$  conversion decreased slightly to ~49%, and CO conversion was measured at about 70%, being lower than that under the thermal condition (which was close to 100%). By increasing the CO concentration in the feed gas (*i.e.*,  $\text{CO}/\text{CO}_2 = 0.5, 1.0$  and 2.0, respectively), a decrease in  $\text{CO}_2$  conversions was measured (due to the change of gas composition); however, catalyst deactivation was insignificant since the carbon conversion remained stable in stream during the cofeeding tests. More importantly, the catalyst activity regarding  $\text{CO}_2$  conversion and  $\text{CH}_4$  production in  $\text{CO}_2$  hydrogenation can be totally recovered when the system was switched back to the CO-free feed, regardless of the previous CO concentration in the feed, confirming that (i) NTP could be able to completely regenerate the catalyst and (ii) NTP is able to mitigate CO poisoning on  $\text{CO}_2$  hydrogenation (Figure S12b). Interestingly, under NTP conditions, in comparison with ~100% CO conversions under the thermal condition, CO conversions increased from 70 to 92% with an increase in the inlet  $\text{CO}/\text{CO}_2$  ratio from 0.25 to 2. This suggested that the reasons for the decrease in  $\text{CO}_2$  conversion in both systems may be different. As discussed above, in thermal catalysis, preferred CO adsorption on the Ru surface and the subsequent CO hydrogenation prevailed, causing the reduction of the  $\text{CO}_2$  conversion and almost 100% CO conversion. Conversely, under NTP conditions, the plasma could activate the  $\text{CO}_2$  molecules in the gas phase and the vibrationally excited  $\text{CO}_2$  could adsorb on the catalyst surface with lower energy barriers, which facilitated the adsorption of  $\text{CO}_2$  on the catalyst surface.<sup>14</sup> Additionally, the collision of reactive plasma species (such as the vibrationally excited  $\text{CO}_2$  and the excited state of CO, H, OH, and CH in the gas phase according to OES and FTIR<sup>9,25,39</sup>) might help remove the strongly adsorbed surface  $\text{CO}_{\text{ad}}$  and then release the active sites for adsorption.<sup>14,40,41</sup> Thus, NTP alleviated CO adsorption and facilitated  $\text{CO}_2$  adsorption, which result in lower CO conversions and higher  $\text{CO}_2$  conversions than those in the thermal catalysis.

The superiority of the NTP-catalysis over the thermal counterpart, regarding the maintenance and regeneration of the catalyst activity, was proved by the long-term CO poisoning study in Figure 5. At 330 °C, the deterioration of the catalyst performance with the presence of CO in the feed was evident during the 9 h test. Specifically,  $\text{CO}_2$  and CO

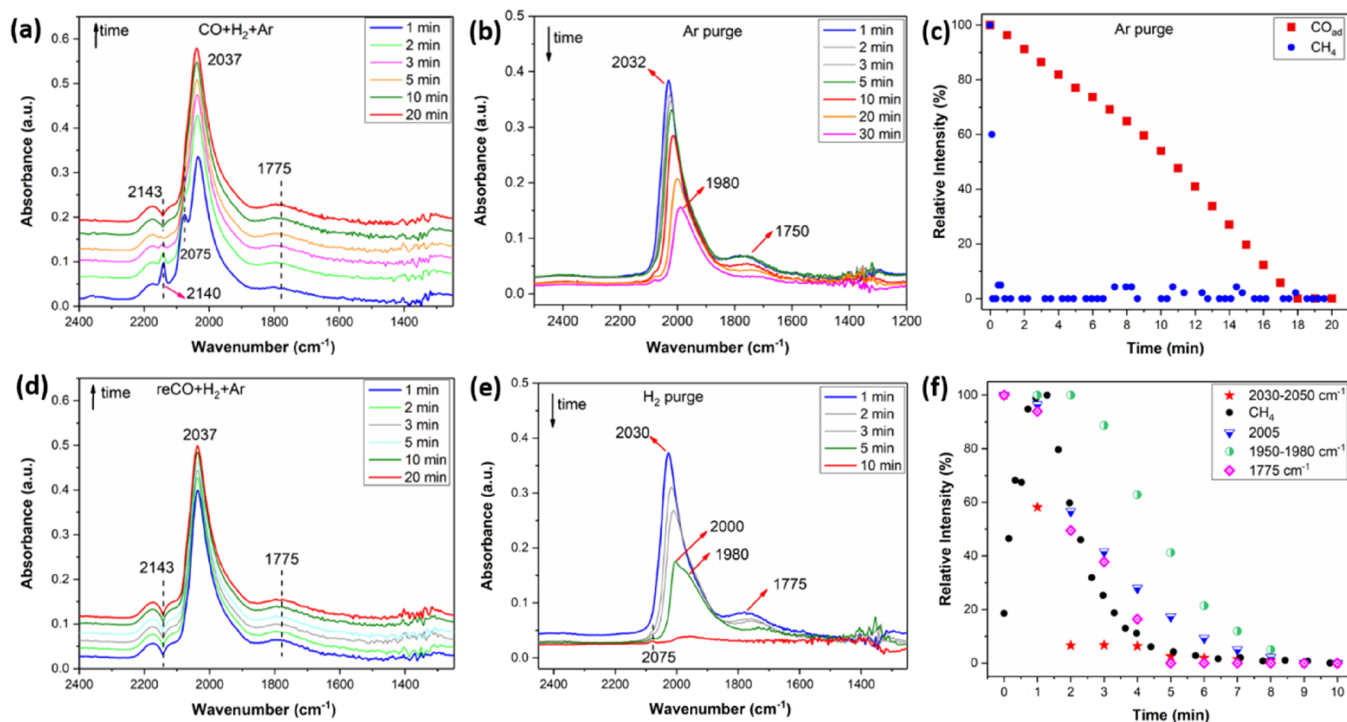


**Figure 6.** *In situ* DRIFTS spectra of surface species collected at 250 °C in the thermally activated CO hydrogenation over the Ru/SiO<sub>2</sub> catalyst. (a) Initial feed composition: 3% CO + 9% H<sub>2</sub> + Ar; (b) change to inert Ar; (c) variations of CO<sub>ad</sub> intensity from *in situ* DRIFTS and CH<sub>4</sub> intensity from MS after switching to Ar at 250 °C; (d) change back to the feed: 3% CO + 9% H<sub>2</sub> + Ar; (e) change to H<sub>2</sub>/Ar; (f) variations of CO<sub>ad</sub> intensity from *in situ* DRIFTS and CH<sub>4</sub> intensity from MS after switching the feed to H<sub>2</sub>/Ar at 250 °C.

conversions (Figure 5a) and CH<sub>4</sub> formation (Figure S13a) dropped by about 42, 7, and 15%, respectively. By removing CO from the feed (ToS = 640–790 min in Figure 5a), CO<sub>2</sub> conversion and CH<sub>4</sub> production over Ru/SiO<sub>2</sub> were recovered to ~93 and ~87% only. Considering that flowing inert gases at high temperature could be used to recover the catalyst reactivity, the deactivated catalyst was regenerated *in situ* at 330 °C by sweeping with Ar for 3.5 h, trying to remove the strongly adsorbed surface species from the catalyst surface. However, as shown in Figure 5a and Figure S13a, the deactivation of catalyst due to CO poisoning under the thermal condition was permanent. Previous theoretical and experimental studies<sup>42,43</sup> suggested that the CO molecule could block the active sites for CO<sub>2</sub> and H<sub>2</sub> adsorption, thus decreasing the dissociated H<sub>ad</sub> on the Ru surface and consequently leading to the deposition of surface carbon species and metal sintering. Conversely, in NTP-catalysis (at 6.5 kV), the catalyst presented stable performance over 9 h, with the constant CO<sub>2</sub> conversion at about 38% and decreased CO conversion (by about 6%). Furthermore, after returning to the CO-free feed (ToS = 640–790 min, Figure 5b), the CO<sub>2</sub> conversion was recovered to ~53% slowly (being comparable with that of the fresh catalyst at ToS = 0–100 min). During the same period (ToS = 640–790 min in Figure S13b), the corresponding CH<sub>4</sub> production decreased to the initial level, confirming that NTP could recover the performance of the catalyst. The recovery trend of CO<sub>2</sub> conversion and CH<sub>4</sub> production was attributed to the consumption of residual adsorbed carbon species under NTP, thus regenerating active sites available for CO<sub>2</sub> hydrogenation. The catalyst was further treated *in situ* under Ar and NTP (at 4.0 kV) for 30 min (ToS = 790–820 min, as shown in Figure 5b). After that, NTP-activated CO<sub>2</sub> hydrogenation was performed again with the

CO-free feed (ToS = 829–945 min in Figure 5b), and the NTP-catalysis system showed the fully recovered performance. The corresponding TEM analysis of the catalysts after the long-term deactivation test (Figure S14) showed the metal sintering of the catalyst in thermal catalysis; that is, the Ru particle size increased from ~1.6 to ~3.1 nm after the thermal catalysis. Conversely, the Ru particle size showed no significant changes after the NTP-catalysis, confirming the antisintering ability of the hybrid system.

**3.4. Mechanisms of CO Poisoning.** To understand CO poisoning in the catalysis, comparative *in situ* DRIFTS–MS studies were carried out and compared with the DRIFTS study of CO<sub>2</sub> hydrogenation in Figure 3 and Figure S7. Under the thermal condition, the DRIFTS spectra measured with CO/H<sub>2</sub> mixture (Figure 6a,c) showed that the intensity of the carbonyl bands was significantly enhanced compared with the case of CO<sub>2</sub> hydrogenation (Figure S7), suggesting the relatively strong CO binding with the Ru surface. Specifically, in addition to the gas-phase CO band (at ~2143 cm<sup>-1</sup>), the broad carbonyl bands in a range of 2140–1770 cm<sup>-1</sup> can be deconvoluted into three kinds of CO<sub>ad</sub> bonds, *i.e.*, the bands at 1775 and 1950–1980 cm<sup>-1</sup> (for the bridged carbonyls), 2005 cm<sup>-1</sup> (for the linearly adsorbed CO with monobinding configuration), and 2030–2075 cm<sup>-1</sup> (for the linearly adsorbed CO with multiple-binding configuration).<sup>30</sup> After changing the feed to inert Ar (Figure 6b,c), the CO<sub>ad</sub> bands decreased much slower than that in CO<sub>2</sub> hydrogenation (Figure S7b), indicating that more strongly adsorbed carbonyl species formed on the surface when CO was in the feed. By switching the feed to H<sub>2</sub> (Figure 6e,f), surface carbonyl species disappeared within 10 min, and the CH<sub>4</sub> concentration at the outlet of the DRIFTS cell showed a maximum (at ~1.3 min, which was followed by a continuous decline until zero),

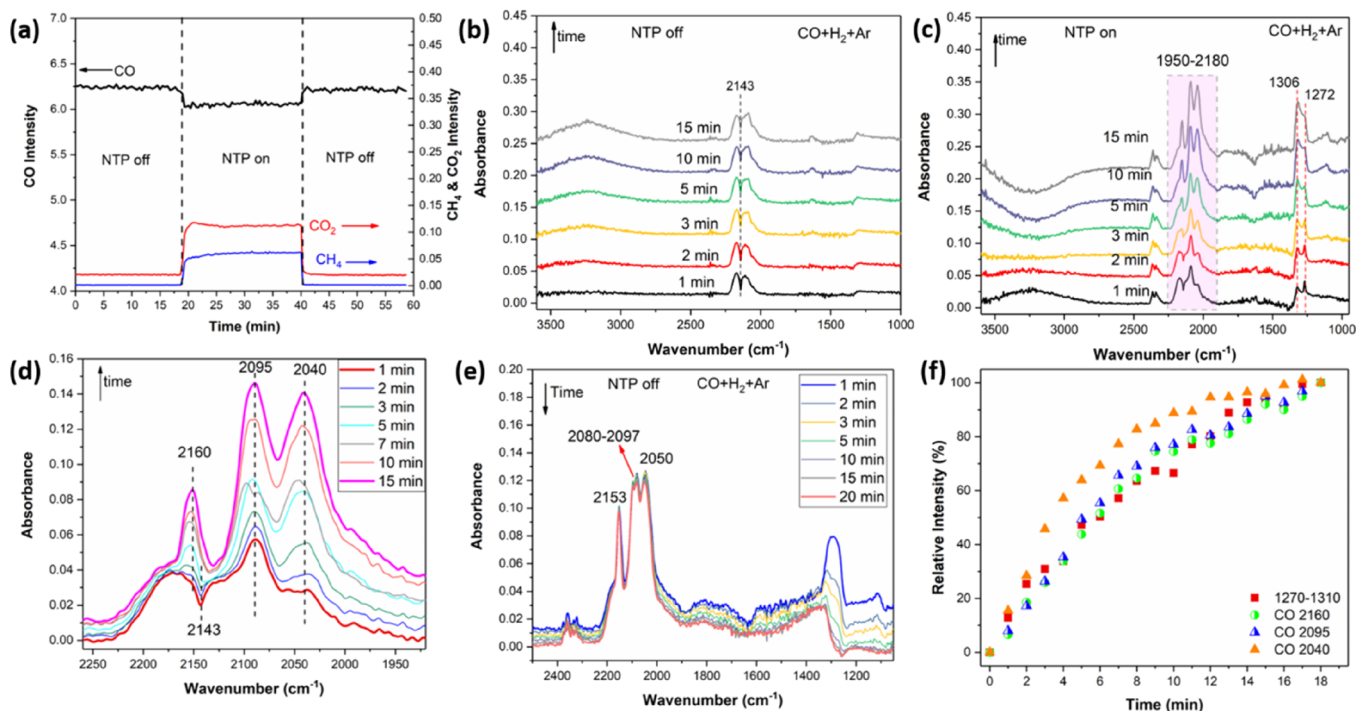


**Figure 7.** (a) Corresponding MS signals collected simultaneously from the DRIFTS cell as a function of time during the NTP-assisted CO hydrogenation over the Ru/SiO<sub>2</sub> catalyst. *In situ* DRIFTS spectra of surface species for CO hydrogenation over the Ru/SiO<sub>2</sub> catalyst under (b) the NTP-off condition with the feed gas of 3% CO + 9% H<sub>2</sub> + Ar, (c, d) NTP-on condition with the feed gas (at 5.5 kV and 27.0 kHz), and (e) NTP-off condition with the feed gas. (f) Relative intensities of surface species as a function of ToS recorded in the *in situ* DRIFTS from (c) and (d) during CO hydrogenation under NTP (at 5.5 kV and 27.0 kHz).

showing that the adsorbed CO was converted to CH<sub>4</sub> in the presence of H<sub>2</sub>. The evolution of the respective surface species as a function of time (Figure 6f) showed that the intensity of the carbonyl group at 2030–2050 cm<sup>-1</sup> quickly decayed (within 2 min) under H<sub>2</sub>, being the most reactive surface species, while the bridged carbonyl at 1775 cm<sup>-1</sup> and linear monocarbonyl at 2005 cm<sup>-1</sup> disappeared completely with comparatively slow rates. In contrast, the intensity of the peak at 1950–1980 cm<sup>-1</sup>, corresponding to geminal dicarbonyls adsorbed on the low coordination Ru sites, remained constant within the initial 2 min and then decreased slowly, being relatively stable on the Ru surface and less reactive for hydrogenation.<sup>44</sup> The presence of these stable and less reactive surface species might block the active sites and hence contributed to the catalyst deactivation. Based on the findings from *in situ* DRIFTS–MS, one can conclude that, under the thermal condition, CO hydrogenation proceeded with similar pathways to those of the catalytic CO<sub>2</sub> hydrogenation.<sup>45</sup> However, the strong adsorption of CO on the catalyst surface could saturate the active sites, inhibiting CO<sub>2</sub> and H<sub>2</sub> adsorption.

With the CO<sub>2</sub> + CO + H<sub>2</sub> feed under the thermal condition, the associated DRIFTS spectra showed the combined features of the CO<sub>2</sub>/CO-alone hydrogenation system (as shown in Figure S15a,c), which was substantiated by the presence of strongly adsorbed CO<sub>ad</sub> and C<sub>x</sub>H<sub>y</sub> species on the surface. After the introduction of CO into the feed, CO coverage increased significantly and could not be completely removed by Ar sweeping (Figure S15d), indicating that the strongly adsorbed CO<sub>ad</sub> occupied the active sites for CO<sub>2</sub> and H<sub>2</sub> adsorption. Accordingly, based on the findings obtained from the thermal catalysis and relevant *in situ* DRIFTS characterization, it was

plausible that the presence of CO in the system produced strongly adsorbed CO species on the Ru sites, which inhibited both CO<sub>2</sub> and H<sub>2</sub> adsorption, thus suppressing CO<sub>2</sub> hydrogenation. Due to the limited concentration of surface H<sub>ad</sub> species, the relatively stable and inactive carbon-containing species, such as carbonyl deposition, were encouraged to be formed on the catalyst surface, and they might progressively block the active sites. Thus, the associated carbonaceous species deposition and metal sintering lead to the permanent catalyst deactivation,<sup>46</sup> which confirms the results in Figures 4a and 5a.

Without plasma discharge at RT, the Ru/SiO<sub>2</sub> catalyst showed no activity for CO hydrogenation, that is, (i) no CO conversion by MS as shown in Figure 7a and (ii) the only presence of gas-phase CO (at ~2143 cm<sup>-1</sup>) according to DRIFTS (Figure 7b). Upon the ignition of NTP, the MS profiles (Figure 7a) showed the instant decrease of CO signal and simultaneous increase of CO<sub>2</sub> and CH<sub>4</sub> signals, confirming the production of CH<sub>4</sub> and CO<sub>2</sub> in the NTP-catalysis. CO<sub>2</sub> formation was due to WGS, which could be activated by NTP.<sup>5</sup> Water was the product from the NTP-activated catalytic CO hydrogenation. As discussed above (Figure 4b), when CO was introduced into the feed for NTP-activated CO<sub>2</sub> hydrogenation, a decrease in CO<sub>2</sub> conversion was measured, which might be partly caused by the water-gas shift reaction. Simultaneously, the gas-phase CO<sub>2</sub> peak at about 2350 cm<sup>-1</sup> was measured by DRIFTS (Figure 7c), in line with the intensity change from MS. In the OCO region (Figure 7c,d), the peak for gas-phase CO at 2143 cm<sup>-1</sup> disappeared, and the continuous development of the IR bands at 2095 and 2160 cm<sup>-1</sup> could be attributed to the linearly adsorbed carbonyl species on Ru<sup>δ+</sup> with Ru<sup>δ+</sup>-CO and Ru<sup>δ+</sup>-(CO)<sub>n</sub> configurations,

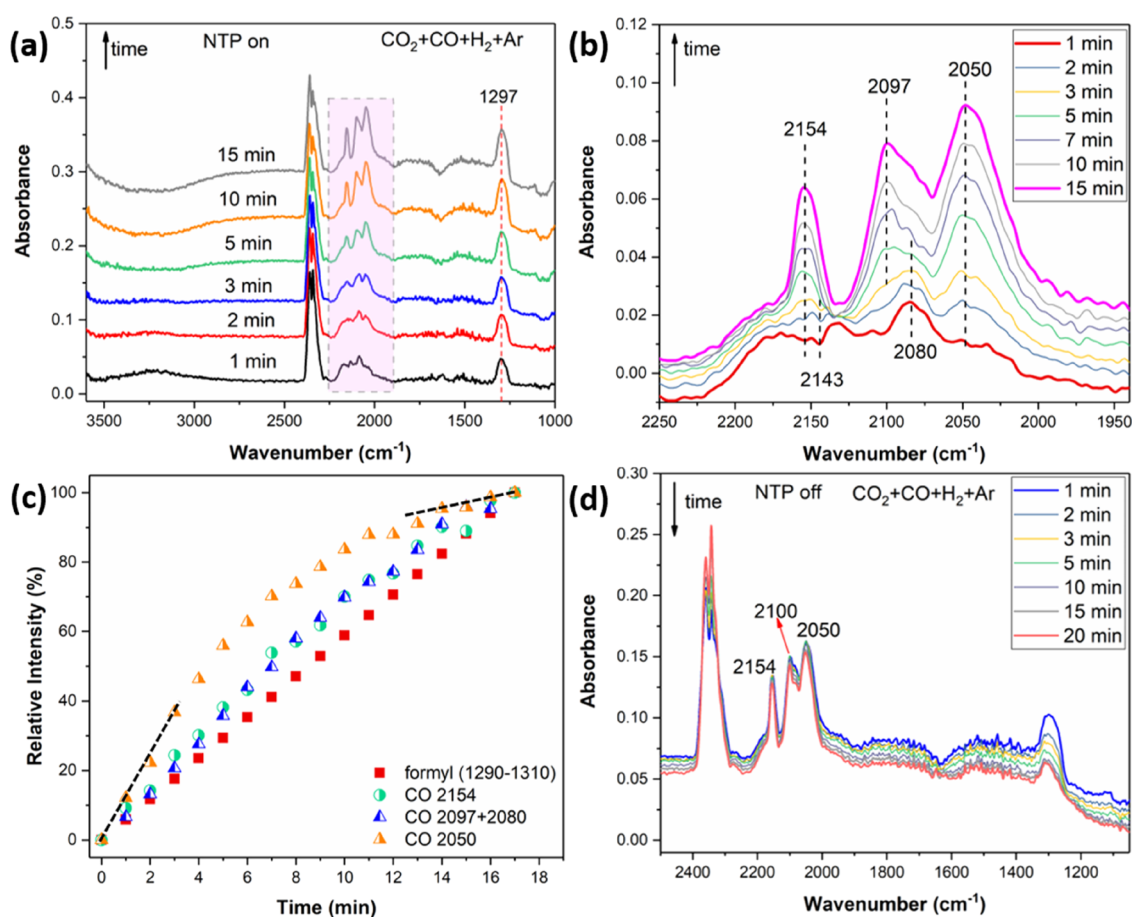


**Figure 8.** *In situ* DRIFTS spectra of surface species for hydrogenation of  $\text{CO}_2/\text{CO}$  over the  $\text{Ru}/\text{SiO}_2$  catalyst under (a, b) the NTP-on condition with the feed gas of 1.5%  $\text{CO}_2$  + 1.5%  $\text{CO}$  + 9%  $\text{H}_2$  + Ar (at 5.5 kV and 27.0 kHz), (c) relative intensities of surface species as a function of ToS recorded in the *in situ* DRIFTS from (a) and (b), and (d) NTP-off condition with the feed gas.

respectively. Another characteristic peak at  $2040\text{ cm}^{-1}$  was assigned to the CO linearly adsorbed on  $\text{Ru}^0$ , while the gradually increased peaks at about  $1272$  and  $1306\text{ cm}^{-1}$  corresponded to formyl species ( $\text{CH}_2\text{O}$ ). The evolution of the surface carbon species recorded by DRIFTS as a function of time is correlated (Figure 7f). The increasing rate of carbonyl bands at  $2095$  and  $2160\text{ cm}^{-1}$  was comparable with that of formyl species, which supported the fact that CO is the intermediate toward formyl species. Also, the formation rate of  $\text{CO}_{\text{ad}}$  band at  $2040\text{ cm}^{-1}$  increased relatively fast, which might be due to  $\text{CO}_2$  dissociation (formed by water-gas shift reaction) and CO adsorption. By switching off NTP, the peak of the gas-phase  $\text{CO}_2$  decreased quickly, and the system was not active again for CO hydrogenation, which was in good agreement with the MS profile. Regarding the carbon species, the formyl species disappeared gradually due to desorption after the extinction of plasma (Figure S16), while  $\text{CO}_{\text{ad}}$  band intensity barely changed, indicating the strong interaction between the  $\text{CO}_{\text{ad}}$  species and catalyst surface. Furthermore, when the feed was switched to  $\text{H}_2/\text{Ar}$  (from 3%  $\text{CO}$  + 9%  $\text{H}_2$  + Ar), DRIFTS characterization (Figure S17a) showed that the surface  $\text{CO}_{\text{ad}}$  species at  $2090\text{ cm}^{-1}$  (due to gas-phase CO adsorption) decreased immediately, while the intensity of formyl species increased initially and then decreased slowly. The initial increase of the formyl species on the catalyst surface could be ascribed to the reaction between  $\text{CO}_{\text{ad}}$  and  $\text{H}_{\text{ad}}$  (to form the formyl), while the subsequent decrease of the formyl

species was due to the consumption of residual formyl species to form  $\text{CH}_4$ . As shown in Figure S17b, the rate of decrease of formyl species and  $\text{CH}_4$  concentration (at the outlet of the DRIFTS cell by MS) was similar, confirming that the formyl species originated from the reaction between  $\text{CO}_{\text{ad}}$  and  $\text{H}_{\text{ad}}$  and were the active intermediate for  $\text{CH}_4$  formation. DRIFTS analysis of CO hydrogenation under the NTP condition showed that CO hydrogenation to  $\text{CH}_4$  proceeded via CO adsorption and the formyl pathway, being similar with that of  $\text{CO}_2$  hydrogenation (Figure 3).

NTP-catalysis with the  $\text{CO}_2/\text{CO}/\text{H}_2$  feed was examined by DRIFTS-MS (Figure 8 and Figure S18). Being different from CO hydrogenation, the  $\text{CO}_{\text{ad}}$  peak at  $2080\text{ cm}^{-1}$ , due to  $\text{CO}_2$  dissociation, appeared first and then combined with the peak at  $2097\text{ cm}^{-1}$  (originating from the gas-phase CO adsorption). Accordingly, the evolution profile of the surface carbon species (Figure 8c) showed that the  $\text{CO}_{\text{ad}}$  species had higher increasing rates than that of formyl species initially (within 8 min) due to  $\text{CO}_2$  dissociation and CO adsorption on the Ru sites. The subsequent change in the increasing rate was due to saturation of relevant active sites on the Ru surface by  $\text{CO}_2/\text{CO}$  adsorption.<sup>30</sup> This finding suggested that  $\text{CO}_2$  and CO coadsorption existed in the NTP-catalysis. In contrast, the formyl species presented a constant formation rate, confirming that the formyl species originated from the reaction between  $\text{CO}_{\text{ad}}$  and  $\text{H}_{\text{ad}}$ . In addition, by switching CO feed on and off alternatively, DRIFTS-MS characterization of the catalysis

(Figure S19) showed that the CO<sub>2</sub> MS signal increased with CO in the feed (*i.e.*, production of CO<sub>2</sub>), which confirms the presence of WGS under the NTP condition with the CO<sub>2</sub>/CO/H<sub>2</sub> mixture. Therefore, under NTP conditions, the presence of CO in the feed affected CO<sub>2</sub> conversions, which was due to (i) the occurrence of WGS in the system for CO<sub>2</sub> formation and (ii) the relatively strong adsorption of CO, in line with the result in Figure 4b. Based on the *in situ* DRIFTS characterization and relevant discussion, the presence of CO in the feed did not alter the reaction pathways for CO<sub>2</sub> hydrogenation under thermal and NTP conditions. However, in comparison with the CO poisoning under the thermal conditions (as discussed before, *i.e.*, due to strong CO adsorption and associated metal sintering of the catalyst), the collisions between reactive plasma-derived species in NTP could recover the active sites by removing the adsorbed carbon species effectively, which lead to the sites available for CO<sub>2</sub> adsorption.<sup>40,41,47</sup> This is confirmed by the comparison of the relevant IR spectra (Figure S20), which showed the comparatively low intensity of the adsorbed CO<sub>ad</sub> on the Ru catalyst under NTP. Therefore, NTP-catalysis promoted the adsorption of CO<sub>2</sub> and alleviated CO adsorption on the catalyst surface in the presence of CO, mitigating the CO poisoning effect on the performance of CO<sub>2</sub> hydrogenation and being opposite to that experienced by the thermal catalysis. More importantly, according to the literature,<sup>48–50</sup> H<sub>2</sub>O molecules will occupy the active sites and present an inhibiting effect on the CO<sub>2</sub> hydrogenation. Conversely, NTP enabled WGS of CO with the produced H<sub>2</sub>O, which shifted the equilibrium of CO<sub>2</sub> hydrogenation toward CH<sub>4</sub> production. The phenomenon observed in the system under investigation showed the interesting effect of CO on NTP-catalytic CO<sub>2</sub> hydrogenation, that is, as a reaction promoter rather than a catalyst poison, due to the copresence of WGS, CO<sub>2</sub> hydrogenation, and CO hydrogenation under NTP conditions.

#### 4. CONCLUSIONS

In this study, the NTP-catalysis system was demonstrated to be efficient for CO<sub>2</sub> hydrogenations under atmospheric conditions, in which 65% CO<sub>2</sub> conversion and 63% CH<sub>4</sub> yield can be achieved over the Ru/SiO<sub>2</sub> catalyst. Also, the intrinsic nature of catalyst such as surface area is crucial under both thermal and NTP conditions. The comparative kinetic and *in situ* DRIFTS–MS study revealed that the NTP-catalysis could lower the energy barrier required for catalysis and enable both Langmuir–Hinshelwood and Eley–Rideal mechanisms.

The effect of CO on the catalysis under both thermal and NTP conditions was investigated to understand CO poisoning comparatively. In the thermal catalysis, the catalyst suffered from a significant decrease in CO<sub>2</sub> conversion and deactivation due to CO poisoning, while in the NTP-catalysis, the CO played a different role in the system, and the catalyst showed comparatively good stability and regenerability by NTP. *In situ* DRIFTS–MS study of the thermal catalysis showed that (i) CO preferred to adsorb on the Ru surface strongly to inhibit CO<sub>2</sub> and H<sub>2</sub> adsorption and decrease CO<sub>2</sub> conversion significantly and (ii) the formation of less reactive and strongly adsorbed carbon species (*e.g.*, CO<sub>ad</sub>) due to CO strong adsorption and metal sintering deactivates the catalyst permanently. Conversely, in NTP-catalysis, collisions of reactive plasma-derived species contributed to the recovery of the active sites by removing the strongly adsorbed CO<sub>ad</sub>,

which facilitated CO<sub>2</sub> adsorption and, hence, CO<sub>2</sub> hydrogenation. Therefore, NTP-catalysis could alleviate the CO effect on CO<sub>2</sub> hydrogenation and regenerate the catalyst *in situ* in the presence of CO during the catalysis. Importantly, the NTP-induced WGS of CO with the produced H<sub>2</sub>O also promoted the equilibrium shift of CO<sub>2</sub> hydrogenation toward CH<sub>4</sub> production. This work demonstrates that, under NTP conditions, the role played by CO in Ru-catalyzed CO<sub>2</sub> hydrogenation is fundamentally different from its positioning role in thermal catalysis, showing the potential of NTP-catalysis to address some of the challenges in conventional heterogeneous catalysis, specifically, the development of advanced hybrid NTP-catalysis systems to solve the chemical deactivation issues for practical catalysis.

#### ■ ASSOCIATED CONTENT

##### Supporting Information

The Supporting Information is available free of charge at <https://pubs.acs.org/doi/10.1021/acscatal.0c03620>.

Detailed characterization of catalysts; relevant catalyst assessment for catalytic CO<sub>2</sub> hydrogenation; kinetic parameters of the thermal and NTP systems; relevant *in situ* DRIFTS data of the thermal and NTP-catalysis systems (PDF)

#### ■ AUTHOR INFORMATION

##### Corresponding Authors

**Christopher Hardacre** – Department of Chemical Engineering and Analytical Science, School of Engineering, The University of Manchester, Manchester M13 9PL, United Kingdom; [orcid.org/0000-0001-7256-6765](https://orcid.org/0000-0001-7256-6765); Email: [c.hardacre@manchester.ac.uk](mailto:c.hardacre@manchester.ac.uk)

**Xiaolei Fan** – Department of Chemical Engineering and Analytical Science, School of Engineering, The University of Manchester, Manchester M13 9PL, United Kingdom; [orcid.org/0000-0002-9039-6736](https://orcid.org/0000-0002-9039-6736); Email: [xiaolei.fan@manchester.ac.uk](mailto:xiaolei.fan@manchester.ac.uk)

##### Authors

**Shanshan Xu** – Department of Chemical Engineering and Analytical Science, School of Engineering, The University of Manchester, Manchester M13 9PL, United Kingdom

**Sarayute Chansai** – Department of Chemical Engineering and Analytical Science, School of Engineering, The University of Manchester, Manchester M13 9PL, United Kingdom

**Shaojun Xu** – UK Catalysis Hub, Research Complex at Harwell, Didcot OX11 0FA, United Kingdom; Cardiff Catalysis Institute, School of Chemistry, Cardiff University, Cardiff CF10 3AT, United Kingdom; [orcid.org/0000-0002-8026-8714](https://orcid.org/0000-0002-8026-8714)

**Cristina E. Stere** – Department of Chemical Engineering and Analytical Science, School of Engineering, The University of Manchester, Manchester M13 9PL, United Kingdom; [orcid.org/0000-0001-8604-0211](https://orcid.org/0000-0001-8604-0211)

**Yilai Jiao** – Shenyang National Laboratory for Materials Science, Institute of Metal Research, Chinese Academy of Sciences, Shenyang 110016, China

**Sihai Yang** – Department of Chemistry, School of Natural Science, The University of Manchester, Manchester M13 9PL, United Kingdom; [orcid.org/0000-0002-1111-9272](https://orcid.org/0000-0002-1111-9272)

Complete contact information is available at: <https://pubs.acs.org/doi/10.1021/acscatal.0c03620>

## Author Contributions

The manuscript was written through contributions of all authors. All authors have given approval to the final version of the manuscript.

## Notes

The authors declare no competing financial interest.

## ACKNOWLEDGMENTS

S.X. thanks the financial support from the Dean's Doctoral Scholar Awards from the University of Manchester. The UK Catalysis Hub is kindly thanked for resources and support provided via our membership of the UK Catalysis Hub Consortium and funded by EPSRC grant EP/R026939/1, EP/R026815/1, EP/R026645/1, EP/R027129/1, or EP/M013219/1(biocatalysis).

## REFERENCES

- (1) Whitehead, J. C. Plasma-Catalysis: Is It Just a Question of Scale? *Front. Chem. Sci. Eng.* **2019**, *13*, 264–273.
- (2) Neyts, E. C.; Ostrikov, K. K.; Sunkara, M. K.; Bogaerts, A. Plasma Catalysis: Synergistic Effects at the Nanoscale. *Chem. Rev.* **2015**, *115*, 13408–13446.
- (3) Bogaerts, A.; Tu, X.; Whitehead, J. C.; Centi, G.; Lefferts, L.; Guitella, O.; Azzolina-Jury, F.; Kim, H.-H.; Murphy, A. B.; Schneider, W. F.; Nozaki, T.; Hicks, J. C.; Rousseau, A.; Thevenet, F.; Khacef, A.; Carreon, M. The 2020 Plasma Catalysis Roadmap. *J. Phys. D: Appl. Phys.* **2020**, *53*, 443001.
- (4) Vakili, R.; Gholami, R.; Stere, C. E.; Chansai, S.; Chen, H.; Holmes, S. M.; Jiao, Y.; Hardacre, C.; Fan, X. Plasma-Assisted Catalytic Dry Reforming of Methane (DRM) over Metal-Organic Frameworks (MOFs)-Based Catalysts. *Appl. Catal., B* **2020**, *260*, 118195.
- (5) Stere, C. E.; Anderson, J. A.; Chansai, S.; Delgado, J. J.; Goguet, A.; Graham, W. G.; Hardacre, C.; Taylor, S. F. R.; Tu, X.; Wang, Z.; Yang, H. Non-Thermal Plasma Activation of Gold-Based Catalysts for Low-Temperature Water-Gas Shift Catalysis. *Angew. Chem., Int. Ed.* **2017**, *56*, 5579–5583.
- (6) Xu, S.; Chansai, S.; Stere, C.; Inceesungvorn, B.; Goguet, A.; Wangkawong, K.; Taylor, S. F. R.; Al-Janabi, N.; Hardacre, C.; Martin, P. A.; Fan, X. Sustaining Metal–Organic Frameworks for Water-Gas Shift Catalysis by Non-Thermal Plasma. *Nat. Catal.* **2019**, *2*, 142–148.
- (7) Chen, H.; Mu, Y.; Shao, Y.; Chansai, S.; Xu, S.; Stere, C. E.; Xiang, H.; Zhang, R.; Jiao, Y.; Hardacre, C.; Fan, X. Coupling Non-Thermal Plasma with Ni Catalysts Supported on Beta Zeolite for Catalytic CO<sub>2</sub> Methanation. *Catal. Sci. Technol.* **2019**, *9*, 4135–4145.
- (8) Kim, J.; Go, D. B.; Hicks, J. C. Synergistic Effects of Plasma-Catalyst Interactions for CH<sub>4</sub> Activation. *Phys. Chem. Chem. Phys.* **2017**, *19*, 13010–13021.
- (9) Xu, S.; Chansai, S.; Shao, Y.; Xu, S.; Wang, Y.-c.; Haigh, S.; Mu, Y.; Jiao, Y.; Stere, C. E.; Chen, H.; Fan, X.; Hardacre, C. Mechanistic Study of Non-Thermal Plasma Assisted CO<sub>2</sub> Hydrogenation over Ru Supported on MgAl Layered Double Hydroxide. *Appl. Catal., B* **2020**, *268*, 118752.
- (10) Chen, H.; Goodarzi, F.; Mu, Y.; Chansai, S.; Mielby, J. J.; Mao, B.; Sooknoi, T.; Hardacre, C.; Kegnaes, S.; Fan, X. Effect of Metal Dispersion and Support Structure of Ni/Silicalite-1 Catalysts on Non-Thermal Plasma (NTP) Activated CO<sub>2</sub> Hydrogenation. *Appl. Catal., B* **2020**, *272*, 119013.
- (11) Gupta, N. M.; Londhe, V. P.; Kamble, V. S. Gas-Uptake, Methanation, and Microcalorimetric Measurements on the Coadsorption of CO and H<sub>2</sub> over Polycrystalline Ru and a Ru/TiO<sub>2</sub> Catalyst. *J. Catal.* **1997**, *169*, 423–437.
- (12) Falbo, L.; Visconti, C. G.; Lietti, L.; Szanyi, J. The Effect of CO on CO<sub>2</sub> Methanation over Ru/Al<sub>2</sub>O<sub>3</sub> Catalysts: A Combined Steady-State Reactivity and Transient DRIFT Spectroscopy Study. *Appl. Catal., B* **2019**, *256*, 117791.
- (13) Barboun, P.; Mehta, P.; Herrera, F. A.; Go, D. B.; Schneider, W. F.; Hicks, J. C. Distinguishing Plasma Contributions to Catalyst Performance in Plasma-Assisted Ammonia Synthesis. *ACS Sustainable Chem. Eng.* **2019**, *7*, 8621–8630.
- (14) Whitehead, J. C. Plasma–Catalysis: The Known Knowns, the Known Unknowns and the Unknown Unknowns. *J. Phys. D: Appl. Phys.* **2016**, *49*, 243001.
- (15) Gibson, E. K.; Stere, C. E.; Curran-McAteer, B.; Jones, W.; Cibir, G.; Gianolio, D.; Goguet, A.; Wells, P. P.; Catlow, C. R. A.; Collier, P.; Hinde, P.; Hardacre, C. Probing the Role of a Non-Thermal Plasma (NTP) in the Hybrid NTP Catalytic Oxidation of Methane. *Angew. Chem., Int. Ed.* **2017**, *56*, 9351–9355.
- (16) Mei, D.; Zhu, X.; He, Y.-L.; Yan, J. D.; Tu, X. Plasma-Assisted Conversion of CO<sub>2</sub> in a Dielectric Barrier Discharge Reactor: Understanding the Effect of Packing Materials. *Plasma Sources Sci. Technol.* **2014**, *24*, No. 015011.
- (17) Mehta, P.; Barboun, P.; Go, D. B.; Hicks, J. C.; Schneider, W. F. Catalysis Enabled by Plasma Activation of Strong Chemical Bonds: A Review. *ACS Energy Lett.* **2019**, *4*, 1115–1133.
- (18) Zhang, Y.; Wang, H.-y.; Jiang, W.; Bogaerts, A. Two-Dimensional Particle-in Cell/Monte Carlo Simulations of a Packed-Bed Dielectric Barrier Discharge in Air at Atmospheric Pressure. *New J. Phys.* **2015**, *17*, No. 083056.
- (19) Zhang, K.; Zhang, G.; Liu, X.; Phan, A. N.; Luo, K. A Study on CO<sub>2</sub> Decomposition to CO and O<sub>2</sub> by the Combination of Catalysis and Dielectric-Barrier Discharges at Low Temperatures and Ambient Pressure. *Ind. Eng. Chem. Res.* **2017**, *56*, 3204–3216.
- (20) Zhang, Y.; Wang, H.-y.; Zhang, Y.-r.; Bogaerts, A. Formation of Microdischarges inside a Mesoporous Catalyst in Dielectric Barrier Discharge Plasmas. *Plasma Sources Sci. Technol.* **2017**, *26*, No. 054002.
- (21) Weatherbee, G. D.; Bartholomew, C. H. Hydrogenation of CO<sub>2</sub> on Group VIII Metals: II. Kinetics and Mechanism of CO<sub>2</sub> Hydrogenation on Nickel. *J. Catal.* **1982**, *77*, 460–472.
- (22) Prairie, M. R.; Renken, A.; Highfield, J. G.; Thampi, K. R.; Grätzel, M. A Fourier Transform Infrared Spectroscopic Study of CO<sub>2</sub> Methanation on Supported Ruthenium. *J. Catal.* **1991**, *129*, 130–144.
- (23) Solymosi, F.; Erdöhelyi, A.; Kocsis, M. Methanation of CO<sub>2</sub> on Supported Ru Catalysts. *J. Chem. Soc., Faraday Trans. 1* **1981**, *77*, 1003–1012.
- (24) Kuśmierz, M. Kinetic Study on Carbon Dioxide Hydrogenation over Ru/ $\gamma$ -Al<sub>2</sub>O<sub>3</sub> Catalysts. *Catal. Today* **2008**, *137*, 429–432.
- (25) Azzolina-Jury, F.; Thibault-Starzyk, F. Mechanism of Low Pressure Plasma-Assisted CO<sub>2</sub> Hydrogenation over Ni-USY by Microsecond Time-Resolved FTIR Spectroscopy. *Top. Catal.* **2017**, *60*, 1709–1721.
- (26) Miao, B.; Ma, S. S. K.; Wang, X.; Su, H.; Chan, S. H. Catalysis Mechanisms of CO<sub>2</sub> and CO Methanation. *Catal. Sci. Technol.* **2016**, *6*, 4048–4058.
- (27) Lalinde, J. A. H.; Roongruangsree, P.; Ilsemann, J.; Bäumer, M.; Kopyscinski, J. CO<sub>2</sub> Methanation and Reverse Water Gas Shift Reaction. Kinetic Study Based on in situ Spatially-Resolved Measurements. *Chem. Eng. J.* **2020**, 124629.
- (28) Garbarino, G.; Bellotti, D.; Finocchio, E.; Magistri, L.; Busca, G. Methanation of Carbon Dioxide on Ru/Al<sub>2</sub>O<sub>3</sub>: Catalytic Activity and Infrared Study. *Catal. Today* **2016**, *277*, 21–28.
- (29) Fisher, I. A.; Bell, A. T. A Comparative Study of CO and CO<sub>2</sub> Hydrogenation over Rh/SiO<sub>2</sub>. *J. Catal.* **1996**, *162*, 54–65.
- (30) Eckle, S.; Anfang, H.-G.; Behm, R. J. r. Reaction Intermediates and Side Products in the Methanation of CO and CO<sub>2</sub> over Supported Ru Catalysts in H<sub>2</sub>-Rich Reformate Gases. *J. Phys. Chem. C* **2011**, *115*, 1361–1367.
- (31) Navarro-Jaén, S.; Navarro, J. C.; Bobadilla, L. F.; Centeno, M. A.; Laguna, O. H.; Odriozola, J. A. Size-Tailored Ru Nanoparticles Deposited over  $\gamma$ -Al<sub>2</sub>O<sub>3</sub> for the CO<sub>2</sub> Methanation Reaction. *Appl. Surf. Sci.* **2019**, *483*, 750–761.
- (32) Fajín, J. L. C.; Gomes, J. R. B.; Cordeiro, M. N. D. S. Mechanistic Study of Carbon Monoxide Methanation over Pure and Rhodium- or Ruthenium-Doped Nickel Catalysts. *J. Phys. Chem. C* **2015**, *119*, 16537–16551.

- (33) Liu, C.-j.; Xu, G.-h.; Wang, T. Non-Thermal Plasma Approaches in CO<sub>2</sub> Utilization. *Fuel Process. Technol.* **1999**, *58*, 119–134.
- (34) Gupta, N. M.; Kamble, V. S.; Rao, K. A.; Iyer, R. M. On the Mechanism of CO and CO<sub>2</sub> Methanation over Ru/Molecular-Sieve Catalyst. *J. Catal.* **1979**, *60*, 57–67.
- (35) Utaka, T.; Okanishi, T.; Takeguchi, T.; Kikuchi, R.; Eguchi, K. Water Gas Shift Reaction of Reformed Fuel over Supported Ru Catalysts. *Appl. Catal., A* **2003**, *245*, 343–351.
- (36) Gupta, N. M.; Kamble, V. S.; Iyer, R. M.; Thampi, K. R.; Gratzel, M. FTIR Studies on the CO, CO<sub>2</sub> and H<sub>2</sub> Co-Adsorption over Ru-RuO<sub>x</sub>/TiO<sub>2</sub> Catalyst. *Catal. Lett.* **1993**, *21*, 245–255.
- (37) Zhang, S.-T.; Yan, H.; Wei, M.; Evans, D. G.; Duan, X. Hydrogenation Mechanism of Carbon Dioxide and Carbon Monoxide on Ru(0001) Surface: A Density Functional Theory Study. *RSC Adv.* **2014**, *4*, 30241–30249.
- (38) Mukkavilli, S.; Wittmann, C.; Tavlarides, L. L. Carbon Deactivation of Fischer-Tropsch Ruthenium Catalyst. *Ind. Eng. Chem. Process Des. Dev.* **1986**, *25*, 487–494.
- (39) Mikhail, M.; Wang, B.; Jalain, R.; Cavadias, S.; Tatoulian, M.; Ognier, S.; Gálvez, M. E.; Da Costa, P. Plasma-Catalytic Hybrid Process for CO<sub>2</sub> Methanation: Optimization of Operation Parameters. *React. Kinet., Mech. Catal.* **2018**, *126*, 629–643.
- (40) Wang, L.; Zhao, Y.; Liu, C.; Gong, W.; Guo, H. Plasma Driven Ammonia Decomposition on a Fe-Catalyst: Eliminating Surface Nitrogen Poisoning. *Chem. Commun.* **2013**, *49*, 3787–3789.
- (41) Zhu, B.; Li, X.-S.; Liu, J.-L.; Liu, J.-B.; Zhu, X.; Zhu, A.-M. In-Situ Regeneration of Au Nanocatalysts by Atmospheric-Pressure Air Plasma: Significant Contribution of Water Vapor. *Appl. Catal., B* **2015**, *179*, 69–77.
- (42) Zhao, P.; He, Y.; Cao, D.-B.; Wen, X.; Xiang, H.; Li, Y. W.; Wang, J.; Jiao, H. High Coverage Adsorption and Co-Adsorption of CO and H<sub>2</sub> on Ru(0001) from DFT and Thermodynamics. *Phys. Chem. Chem. Phys.* **2015**, *17*, 19446–19456.
- (43) Diemant, T.; Rauscher, H.; Bansmann, J.; Behm, R. J. Coadsorption of Hydrogen and CO on Well-Defined Pt<sub>35</sub>Ru<sub>65</sub>/Ru(0001) Surface Alloys-Site Specificity Vs. Adsorbate-Adsorbate Interactions. *Phys. Chem. Chem. Phys.* **2010**, *12*, 9801–9810.
- (44) Wang, X.; Hong, Y.; Shi, H.; Szanyi, J. Kinetic Modeling and Transient DRIFTS–MS Studies of CO<sub>2</sub> Methanation over Ru/Al<sub>2</sub>O<sub>3</sub> Catalysts. *J. Catal.* **2016**, *343*, 185–195.
- (45) Cant, N. W.; Bell, A. T. Studies of Carbon Monoxide Hydrogenation over Ruthenium Using Transient Response Techniques. *J. Catal.* **1982**, *73*, 257–271.
- (46) Carballo, J. M. G.; Finocchio, E.; García-Rodríguez, S.; Ojeda, M.; Fierro, J. L. G.; Busca, G.; Rojas, S. Insights into the Deactivation and Reactivation of Ru/TiO<sub>2</sub> During Fischer–Tropsch Synthesis. *Catal. Today* **2013**, *214*, 2–11.
- (47) Saoud, W. A.; Assadi, A. A.; Guiza, M.; Bouzaza, A.; Aboussaoud, W.; Ouederni, A.; Soutrel, I.; Wolbert, D.; Rtimi, S. Study of Synergetic Effect, Catalytic Poisoning and Regeneration Using Dielectric Barrier Discharge and Photocatalysis in a Continuous Reactor: Abatement of Pollutants in Air Mixture System. *Appl. Catal., B* **2017**, *213*, 53–61.
- (48) Aziz, M. A. A.; Jalil, A. A.; Triwahyono, S.; Saad, M. W. A. CO<sub>2</sub> Methanation over Ni-Promoted Mesoporous Silica Nanoparticles: Influence of Ni Loading and Water Vapor on Activity and Response Surface Methodology Studies. *Chem. Eng. J.* **2015**, *260*, 757–764.
- (49) Falbo, L.; Martinelli, M.; Visconti, C. G.; Lietti, L.; Bassano, C.; Deiana, P. Kinetics of CO<sub>2</sub> Methanation on a Ru-Based Catalyst at Process Conditions Relevant for Power-to-Gas Applications. *Appl. Catal., B* **2018**, *225*, 354–363.
- (50) Bacariza, M. C.; Biset-Peiró, M.; Graça, I.; Guilera, J.; Morante, J.; Lopes, J. M.; Andreu, T.; Henriques, C. DBD Plasma-Assisted CO<sub>2</sub> Methanation Using Zeolite-Based Catalysts: Structure Composition-Reactivity Approach and Effect of Ce as Promoter. *J. CO<sub>2</sub> Util.* **2018**, *26*, 202–211.